Copyright notice

It will be published in the IEEE Sensors Journal 11, Pages 1864-1868, Nov. 2015, DOI: 10.1109/JSEN.2015.2500121.

Device-free human sensing and localization in collaborative human-robot workspaces: a case study

Stefano Savazzi, Vittorio Rampa, Federico Vicentini, Matteo Giussani

***Abstract*—Modern robot manufacturing is fostering the implementation of hybrid production systems characterized by human-robot cooperative tasks. Safety technologies for workers protection require advanced sensing capabilities and flexible solutions that are able to monitor the movements of the operator in proximity of moving robots. This paper proposes the use of wireless device-free localization (DFL) methods and architectures to detect and track a human worker in a cooperative human-robot industrial workspace. The DFL system is composed of groups of massively-interacting small, low-cost, embedded radio-frequency transceivers that perform received power measurements. These devices are anchored in fixed peripheral locations of the plant and provide localization of the worker, who peculiarly carries neither wireless active devices (device-free) nor specific tracking sensors (sensor-free sensing). Operator motion is, in fact, estimated by tracking the perturbations of the radio field induced by the human body, considering the effect of concurrently moving robot as non-stationary interference. The proposed localization and detection algorithm is based on the Jump Linear Markovian System - Interactive Multiple Model method and its positioning accuracy has been validated by experiments performed inside a robotic cell of an industrial test plant. The proposed DFL system has been implemented by employing IEEE 802.15.4 radio-frequency devices operating at 2.4 GHz and integrated into a software safety architecture. Finally, a software toolset has been designed to predict DFL accuracy, to verify experimental measurements and also to support the integration with pre-installed industrial sensors to increase the accuracy of the augmented system.**

I. Introduction

HUMAN-ROBOT cooperation (HRC) plays a dominant role in hybrid production systems [1], [2], where the unchallenged adaptability of human workers is assisted by the flexibility of robots sharing the execution of complex repetitive workflows. Collaborative workspaces, standardized in ISO 10218-2 [3] and using sensor-based safety technology, represent the consolidated new robot manufacturing paradigm [4] where workers protection still remains the most important property. In typical HRC configurations, a robot (e.g. a manipulator for handling or assembling tasks as in Fig. 1) has to interact with a human worker in proximity: interactions of the robot and the operator are often limited according to the collision avoidance constraint that mandates to stop the robot when the distance between robot and operator is below a given security distance [1]. However, in order to efficiently handle more complex cooperative assembly tasks as envisaged in future systems, the human-robot workspace sharing needs to be defined on a level which is much higher than just the avoidance of collision. Further normative efforts are also proceeding with the draft ISO/DTS 15066 [5] that quantitatively clarifies the safety limits for the Speed and Separation Monitoring (SSM) control mode [6]. The crucial factor for safe HRC in SSM mode is therefore the availability of a real-time localization system of a human worker within the workspace [7], possibly obtained by exploiting multiple sensing sources to enable advance human-machine interactions modes. In fact, distributed detection and localization of operators in a large layout can effectively and timely enable some emergency procedures (*e.g.,* speed limitation or motion re-planning).

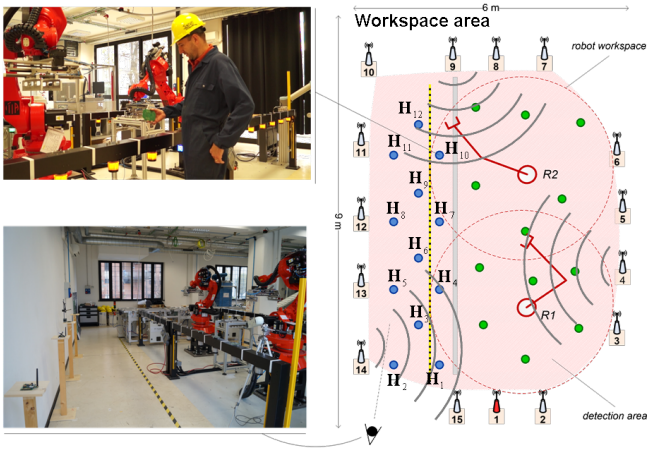

Fig. 1. Reference scenario: (right) layout of a human-shared robotic workspace, with location of wireless nodes (*i.e.,* RF nodes 1-15), ground-truth locations inside the detection area (*i.e.,* circles, some location marked as $\mathbf{H}_i$) and robotic manipulators (*i.e.,* R1, R2); (left) two views of the actual robotic plant used for testing.

Provided that existing industry-standard technology could only partially solve the problem of continuous operator monitoring in the HRC context [6], in this paper, we propose the design and the implementation of a wireless system for the detection and localization of an operator (human sensing) in the context of SSM multi-robot safe applications (see Fig. 1). Most of the research in wireless human sensing and positioning has focused on device-based localization, where a wireless wearable device is attached to a tracked entity and actively participates in the estimation process [8]. However, in the context of robot safety, industrial conditions may be unfit for wearable radio tags. Operators may also find such devices as uncomfortable to wear or carry.

Positioning information can instead be obtained by analyzing the fluctuations, induced by field-obstructing targets [9], of the radio-frequency (RF) electromagnetic waves originated from a dense wireless network. A moving operator, can be localized without wearing specific hardware for motion tracking (sensor-free sensing) nor any active wireless device, resulting in a totally *device-free* localization (DFL) system.

The use of embedded RF nodes for device-free human sensing provides a number of benefits in industrial workspaces [11]

Authors are within the Institute of Electronics, Computer and Telecommunication Engineering (IEIIT) and the Institute of Industrial Technologies and Automation (ITIA) of Italian C.N.R. This work has been carried out in the framework agreement CNR-Regione Lombardia project FIDEAS - "Smart de-manufacturing plants for sustainable and advanced production".

ranging from low cost, node lifetime, and substantial flexibility and scalability with respect to any wired application or system upgrade. In fact, in contrast to other localization systems, the DFL technology adopted here relies on inexpensive commercial radio nodes operating in the unlicensed ISM (Industrial, Scientific and Medical) bands (*e.g.,* 2.4 GHz and 5.8 GHz). In addition, the technology allows to track human body movements by analyzing the perturbations of the same RF field adopted for wireless data transmission and thus leveraging the existing networking infrastructure as a powerful software-defined sensing tool. The DFL system can be therefore adapted to pre-existing networked devices, as deployed around the area of interest at arbitrary locations, that exchange digital information by any industrial communication protocol (*e.g.,* WiFi, ZigBee, WirelessHART, ISA SP100 [10]). With respect to ultra-wide band (UWB) techniques as in [12], the proposed method has the advantage of architectural simplicity, reduced node complexity and limited overall cost. Finally, unlike optical and infrared technologies, RF waves are insensitive to visual obstruction (*e.g.,* due to the presence of fire, smoke or occluding materials) and can also penetrate nonmetallic walls.

A. Related work and original contributions

A few DFL systems are known in literature [9], [11], [12], [13], [14], [15], [16]. The work in [14], for instance, makes use of mean and standard deviation maps of the Received Signal Strength (RSS): these values can be expressed as functions of the target location through a log-normal model. The tomographic method in [9] allows to visually inspect and provide an accurate radio imaging of the area of interest. The work in [15] employs active transmitters as part of the classification system to track human-defined activities or specific postures by analyzing the effects of mobility on RF field. In [16] statistical anomaly detection techniques and particle filtering are applied while the system adapts to small changes in rich multipath environments.

The aim of this paper is to promote the integration of RSS-based DFL technology into an industry-compliant architecture by verifying its ability to support flexible and safe human-robot workspace sharing in a dynamic scenario. In fact, the presence of massive robots, moving inside the shared space, poses new remarkable challenges in signal processing for the implementation of DFL systems, because robots induce large, non-stationary, and very fast RF perturbation effects. In this changing scenario, the environment cannot be considered as static and fingerprinting methods [14], [16] cannot be effectively applied as the contribution of robots to the perturbation of the RF field might cause significant accuracy degradation. The proposed DFL method is not only limited to slowly changing scenarios as in [16], but, with some knowledge about the classes of programmed robot tasks, it is designed to recognize and isolate the effects of possibly fast robot movements. An ad-hoc dynamic Jump Linear Markovian System (JLMS) [17] is proposed to capture the RF perturbations induced by the movements of massive robots, to isolate the RSS perturbations induced by the human body and, finally, to track the operator position in real-time.

The key contributions of the present work can be summarized as: *i*) definition of a set of models that capture the radio propagation effects due to the joint human-robot operational modes in their shared workspace and exploitation of these RSS-based models by using a JLMS framework (Interactive Multiple Model - IMM - method) tailored for the DFL problem; *ii*) design and implementation of a DFL system able to reduce the dynamic effects of the robot movements by effectively recognizing and locating the contribution of the target; *iii*) verification and evaluation of the DFL architecture in a real industrial plant, where the DFL system is devised to be a part of the input component of the Safety Related Parts of the Control System (SRP/CS) [18] that ultimately supervises the robot system safety actions (*e.g.,* reduce speed, stop, resume motion); *iv*) development of a simulation toolset for the purpose of operator localization accuracy prediction, also modeling the impact of system integration/fusion with a pre-installed industry-standard sensor system, herein based on ceiling mounted Time-of-Flight (ToF) cameras.

The paper is organized as follows: Sect. II is dedicated to the definition and validation of the DFL technology herein specifically designed to localize the target while identifying robot movements acting as model-based disturbance. Critical system integration issues, including network set-up, failsafe data processing and practical sensor fusion strategies are discussed in Sect. III focusing on the deployment of DFL technology in a real HRC industrial pilot plant. Experimental results, obtained from a specific IEEE 802.15.4 based implementation of a DFL system, are summarized in Sect. III-C. The simulation toolset described in Sect. IV can be used as a generalized design and development environment for localization accuracy prediction, including the effect of arbitrary network deployments (acquired from calibration data-sets), and accounting for sensor fusion. Finally, Sect. V draws some conclusions and also highlights both potentials and open problems of the DFL technology.

II. Device-free localization and tracking of the operator in a shared workspace

The proposed DFL system is based on a dense wireless mesh network composed of N nodes placed at arbitrary (but known) locations that perform synchronous RSS link measurements. The node locations are either measured during the network deployment phase or self-estimated by the network through a standard device-based localization technique [8]. We model the network as a bidirectional connected graph with N nodes and $L = N\,(N-1)\,/2$ edges (*i.e.,* active bidirectional links) indexed by $\ell \in \mathcal{L} = \{1, \ldots, L\}$. Deployment of wireless nodes must guarantee robust connectivity for all links even in case of obstructions caused by the operator or the robot: this can be obtained by a standard link budget analysis based on a 2D/3D map of the cell. In addition, a post-layout verification stage can be also adopted to minimize coverage holes [19]. The wireless nodes are placed to monitor N_H different locations $\mathbf{H}_i$ $(i = 1, ..., N_H)$ with coordinates $\mathbf{H}_i = [H_{x,i},\, H_{y,i},\, H_{z,i}]$, expressed in a 3D Cartesian robot-centered reference frame, inside an indoor robot workcell. As shown in Fig. 1, the N_H positions $\mathbf{H}_i$ form an ordered set $\mathcal{H} = \{\mathbf{H}_i\}_{i=1}^{N_H}$. This set is selected to track the presence of an operator either inside or at the boundary (*e.g.,* crossing the perimeter) of the detected shared workspace. At time t, the target can therefore be located with consistent position $\mathbf{x}_t = [x_{x,t}, x_{y,t}, x_{z,t}]$ in the surroundings of the locations set $\mathcal{H}$, so that $\mathbf{x}_t \equiv \mathbf{H}_i$. Nonetheless, a target may be also located outside the detection area: this case is indicated as $\mathbf{x}_t = \mathbf{H}_0$. The possible target states are therefore defined as $\mathbf{x}_t \in \{\mathbf{H}_i\}_{i=0}^{N_H} = \bar{\mathcal{H}}$. Having all nodes the same vertical position $H_{z,i} = H_z\, \forall i$, the 3D localization domain reduces to the two-dimensional (2D) space

$\mathcal{X}$ and $\mathbf{x}_t = [x_{x,t}, x_{y,t}] \in \mathcal{X}$.

The investigated setting conforms with a typical HRC scenario: a robotic manipulator (*i.e.,* R1 in Fig. 1) is located inside an open (*i.e.,* fenceless) workspace that is shared with one human worker. In the current configuration, even if several robots are present in the test plant, only one robot (*i.e.,* R1) is tracked since it is the only robotic arm that moves in the shared area. A robot task at time t is described by the state $\boldsymbol{\theta}_t \in \{\mathbf{r}_j\}_{j=0}^{R} = \bar{\boldsymbol{\Theta}}$, where the vectors $\mathbf{r}_j$ denote the current trajectory out of all R robot ones $\boldsymbol{\Theta} = \{\mathbf{r}_j\}_{j=1}^{R}$ in a given region of the workspace (*e.g.,* rotation, translation or roto-translation) while $\mathbf{r}_0$ refers to the absence of robot activity. As detailed in Sect. II-B and III-C, each robot state $\boldsymbol{\theta}_t$ maps into a programmed sequence of movements of the robotic arm over a short time interval $T_R = \max_j \left(T_{R_j}\right)$ where T_{R_j} is the duration of the *j*-th task. Such configuration is fairly common in industrial robot routines [2]. As detailed in Sect. III-A (see also [20] for more details), the wireless network nodes are synchronized through a periodic transmission of IEEE 802.15.4 compliant *beacon-frames* from a network coordinator (NC) acting as sink for remote devices (decoding data frames transmitted by devices) and jointly collecting link RSS measurements for DFL processing. The arrangement should guarantee a fixed RSS sample interval $\Delta t \ll T_R$ small enough for DFL processing using all monitored links.

A single target (*e.g.,* an operator) is assumed to move within the detection area for the purpose of being (anonymously) tracked. During such movements, at discrete time instants $t = 1, 2, 3, \ldots$, the sink node collects the set of L noisy power measurements $\mathbf{s}_t = [s_{1,t} \cdots s_{L,t}]^T$, where each observation $s_{\ell,t}$ represents the RSS measured on the link $\ell \in \mathcal{L}$ during the t-th time interval. The complete set of all measurements up to time t is given by $\mathbf{S}_t = [\mathbf{s}_0, ..., \mathbf{s}_t]^{\mathrm{T}}$. The target position $\mathbf{x}_t$ and the robot configuration (or state) $\boldsymbol{\theta}_t$ are not directly observable since their RF perturbations are merged into the noisy RSS measurements $\mathbf{s}_t$. The problem is to track the joint operator-robot state by using all RF measurements $\mathbf{S}_t$.

The proposed dynamic JLMS framework is designed to estimate and locate the operator position through a real-time system that switches between different DFL propagation models. These models capture the joint human-robot operational modes that are paradigmatic of cooperative tasks in the shared workspace. Although both robot motion and operator movements jointly modify the propagation of the RF waves in a complex way, experimental measurements confirm that the robot has a greater influence on the RF disturbance (due to its typical larger size *w.r.t.* the operator). In addition, the system can be aware of robot trajectories in real time (*e.g.,* through the robot controller, see Sect. III-B). For these reasons, the robot state acts as the JLMS jump parameter for the target tracking. To avoid the exponential complexity of a full jump Markov system processing, a suboptimal multiple model filtering algorithm, *i.e.,* the interacting multiple model (IMM) method [21], is adopted for state estimation.

Fig. 2 provides a schematic overview of the DFL flowchart including an initial off-line model calibration (top) and the on-line continuous target tracking (bottom) from the observed data $\mathbf{S}_t$. The online positioning problem is cast in Sect. II-A into a dynamic state estimation one where the state space can be decomposed into the $N_H + 1$ cell areas describing safe locations of the target interacting with the robot shared space. The target tracking problem corresponds to recursively update

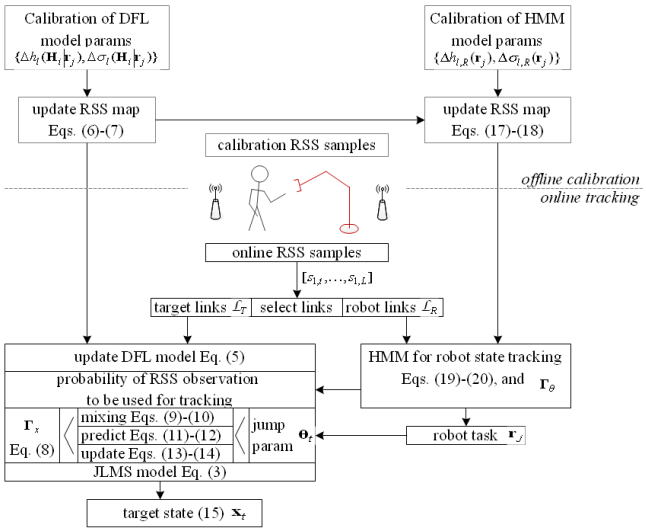

Fig. 2. Flowchart of the DFL algorithm as described in Sect.II.

the a-Posteriori (or belief) probability

$$\Gamma_{\mathrm{x}}(\mathbf{x}_t) = \Pr[\mathbf{x}_t | \mathbf{S}_t] \tag{1}$$

of the operator state $\mathbf{x}_t$ given the data-set of all RSS measurements $\mathbf{S}_t$ and the belief probability of robot state

$$\Gamma_{\theta}(\boldsymbol{\theta}_t) = \Pr[\boldsymbol{\theta}_t | \mathbf{S}_t] \tag{2}$$

as obtained in Sect. II-B. The configuration of the robot activity is thus detected by model likelihoods and Bayesian detection, while each task vector $\mathbf{r}_j$ maps into a different RSS model for DFL and target motion inside the shared space. Target and robot state tracking make use of the optimized wireless link sub-sets $\mathcal{L}_T$ and $\mathcal{L}_R$ designed for target localization and robot state detection, respectively: the selection of $\mathcal{L}_T$,$\mathcal{L}_R \subset \mathcal{L}$ is illustrated below.

A. IMM method for sensor-less tracking of human operator

For target state estimation, we now focus on the subset $\mathcal{L}_T \subseteq \mathcal{L}$ collecting the links that provide the best coverage area for the target position estimation. An optimization of the link subset $\mathcal{L}_T$ is performed to separate the diffraction effects caused by the target from those of the interfering robot. According to the results in [22] for knife-edge objects, the diffraction attenuation of an obstacle is negligible if the distance $d_{\ell,e}$ of its closest edge *w.r.t* the line-of-sight of link ℓ is greater than the maximum value of the Fresnel's radius $\rho_{\ell,\max} = 0.5\sqrt{\lambda d_\ell}$ where d_ℓ is the length of the ℓ-th link: $d_{\ell,e} > \rho_{\ell,\max}$. Therefore, the subset $\mathcal{L}_T$ is selected according to the spatial constraint $\mathcal{L}_T = \{\ell \in \mathcal{L} : d_{\ell,\mathrm{ro}} > \rho_{\ell,\max}\}$, where $d_{\ell,\mathrm{ro}}$ is the distance of the closest edge of the robot during its motion *w.r.t.* the line-of-sight of the ℓ-th link.

Given the measurements $\mathbf{S}_t$ taken over the $\ell \in \mathcal{L}_T$ links up to time t, we consider a discrete JLMS system modeling the evolution of the target state $\mathbf{x}_t$ and the time-varying interaction with the robot, which is in modal state $\boldsymbol{\theta}_t$ due to task execution, as

$$\mathbf{x}_t = g\left(\boldsymbol{\theta}_t\right)\mathbf{x}_{t-1} + f\left(\boldsymbol{\theta}_t\right)\mathbf{v}_t \tag{3}$$

for $t > 1$, with transitional functions $g(\cdot)$ and $f(\cdot)$, and i.i.d process noise sequence $\mathbf{v}_t$. The temporal sequence of

robot states is modeled as a Markov chain with transition probabilities

$$\gamma_{j,k}^{(\theta)} = \Pr[\boldsymbol{\theta}_t = \mathbf{r}_j | \boldsymbol{\theta}_{t-1} = \mathbf{r}_k], \tag{4}$$

with initial probability $\Pr[\boldsymbol{\theta}_0 = \mathbf{r}_0] = 1$ according to the default position $\mathbf{r}_0$ of the robot. The noise sequence $\mathbf{v}_t$ is not Gaussian as it depends on the workspace layout constraints (preventing the use of a Kalman observer for the DFL tracking problem). The robot states and the transition probabilities depend on the specific factory process (e.g. assembly or disassembly tasks) and they can be estimated using the approach illustrated in [17]. Any new robot state $\boldsymbol{\theta}_t = \mathbf{r}_j$ acts as jump Markov parameter that modifies the RSS observation probability to be used for target tracking. Sample $s_{\ell,t}(\mathbf{x}_t|\boldsymbol{\theta}_t = \mathbf{r}_j)$ is thus characterized, $\forall \ell \in \mathcal{L}_T$, in terms of absence (*i.e.,* $\mathbf{x}_t = \mathbf{H}_0$) or presence (*i.e.,* $\mathbf{x}_t = \mathbf{H}_i$) of the target in the covered area and by the robot state $\mathbf{r}_j$; it is

$$\begin{aligned} &s_{\ell,t}(\mathbf{x}_t|\boldsymbol{\theta}_t = \mathbf{r}_j) = \\ &= \begin{cases} h_\ell(\mathbf{H}_0|\mathbf{r}_j) + w_\ell(\mathbf{H}_0|\mathbf{r}_j), & \text{if } \mathbf{x}_t = \mathbf{H}_0 \\ h_\ell(\mathbf{H}_i|\mathbf{r}_j) + w_\ell(\mathbf{H}_i|\mathbf{r}_j), & \text{if } \mathbf{x}_t = \mathbf{H}_i. \end{cases} \end{aligned} \tag{5}$$

For target absent and for the robotic arm configured in state $\mathbf{r}_j$, $h_\ell(\mathbf{H}_0|\mathbf{r}_j)$ and $w_\ell(\mathbf{H}_0|\mathbf{r}_j)$ represent the effects on the RF wave propagation of the fixed obstructions and the time-varying robot-induced RSS fluctuations (fading), respectively. In case of target presence, the measured RSS is affected by an additional perturbation that depends on the specific location $\mathbf{H}_i$. Therefore, both deterministic path-loss $h_\ell(\mathbf{H}_i|\mathbf{r}_j)$ and random fading $w_\ell(\mathbf{H}_i|\mathbf{r}_j) \sim N(0, \sigma_\ell^2(\mathbf{H}_i|\mathbf{r}_j))$ now embed the information about the target location $\mathbf{H}_i$. In particular

$$h_\ell(\mathbf{H}_i|\mathbf{r}_j) = h_\ell(\mathbf{H}_0|\mathbf{r}_0) - \Delta h_\ell(\mathbf{H}_i|\mathbf{r}_j), \tag{6}$$

where $\Delta h_\ell(\mathbf{H}_i|\mathbf{r}_j)$ is the additional variation of attenuation due, for Line-of-Sight (LOS) connections, to the obstruction of the links or, for Non-Line-of-Sight (NLOS) connections, to additional reflections deployed nearby the target position $\mathbf{H}_i$ and subject to the robot state $\mathbf{r}_j$. Moreover, since the operator and the robot can both turn, move or assume different postures in the surrounding of their locations, then an increased RSS variability is observed

$$\sigma_\ell(\mathbf{H}_i|\mathbf{r}_j) = \sigma_\ell(\mathbf{H}_0|\mathbf{r}_0) + \Delta\sigma_\ell(\mathbf{H}_i|\mathbf{r}_j), \tag{7}$$

where $\Delta\sigma_\ell(\mathbf{H}_i|\mathbf{r}_j) \geq 0$ denotes the corresponding increased standard deviation. As shown in Sect. II-C, the evaluation of the 2D connectivity map set $\{\Delta h_\ell(\mathbf{H}_i|\mathbf{r}_j), \Delta\sigma_\ell(\mathbf{H}_i|\mathbf{r}_j)\}$ highlights the perturbations of the RF wavefield compared to the *background state* characterized by the absence of the operator in the detection area. Assuming known both the initial target state probability $\Pr[\mathbf{x}_0] = \Pr[\mathbf{x}_0|\mathbf{S}_0] = \Gamma_{\mathrm{x}}(\boldsymbol{x}_0)$ (*e.g.,* $\Pr[\mathbf{x}_0 = \mathbf{H}_0] = 1$) and the initial default robot position $\mathbf{r}_0$ as $\Pr[\boldsymbol{\theta}_0] = \Pr[\boldsymbol{\theta}_0|\mathbf{S}_0] = \Gamma_\theta(\boldsymbol{\theta}_0)$, we define the mode-conditioned a-Posteriori probability matrix of size $(N_H + 1) \times (R + 1)$

$$\Gamma_{\mathrm{x}}(\mathbf{x}_t|\boldsymbol{\theta}_t) = \Pr[\mathbf{x}_t|\boldsymbol{\theta}_t, \mathbf{S}_t]. \tag{8}$$

The mode-conditioned probability $\Gamma_x(\mathbf{x}_t|\boldsymbol{\theta}_t)$ is iteratively updated by the following three steps as shown below.

Mixing stage. The mixing stage updates the a-Posteriori probability $\Gamma_{\mathrm{x}}(\mathbf{x}_{\mathrm{t}-1}|\boldsymbol{\theta}_{t-1})$ at time $t-1$ to obtain $\Gamma_x(\mathbf{x}_{t-1}|\boldsymbol{\theta}_t)$ based on the robot state transition Eq. (4) and probability $\Gamma_\theta(\boldsymbol{\theta}_{t-1})$. We assume conditional independence between the robot state $\boldsymbol{\theta}_t$ and the target state $\mathbf{x}_{t-1}$ given the previous robot configuration $\boldsymbol{\theta}_{t-1}$. Therefore $\forall j = 0, ..., R$, it is

$$\begin{aligned} &\Gamma_x(\mathbf{x}_{t-1}|\boldsymbol{\theta}_t = \mathbf{r}_j) \propto \\ &\propto \textstyle\sum_{k=0}^{R} \gamma_{j,k}^{(\theta)} \, \Gamma_x(\mathbf{x}_{t-1}|\boldsymbol{\theta}_{t-1} = \mathbf{r}_k) \, \Gamma_\theta(\boldsymbol{\theta}_{t-1} = \mathbf{r}_k). \end{aligned} \tag{9}$$

A more practical decision-directed approach can be implemented to allow for dynamic pruning of the candidate robot states. State pruning is based on the maximum a-Posteriori (MAP) estimate $\hat{\boldsymbol{\theta}}_t$

$$\hat{\boldsymbol{\theta}}_t = \underset{\boldsymbol{\theta}_t \in \bar{\Theta}}{\operatorname{argmax}} \Gamma_\theta(\boldsymbol{\theta}_t), \tag{10}$$

such that $\Gamma_{\mathrm{x}}(\mathbf{x}_{\mathrm{t}}|\hat{\boldsymbol{\theta}}_t) = \Pr[\mathbf{x}_t|\hat{\boldsymbol{\theta}}_t, \mathbf{S}_t]$. Pruning of robot states is thus obtained as $\Gamma_x(\mathbf{x}_{t-1}|\boldsymbol{\theta}_t) = 0$ if $\boldsymbol{\theta}_t \neq \hat{\boldsymbol{\theta}}_t$. Alternatively, another choice is to impose $\Gamma_x(\mathbf{x}_{t-1}|\boldsymbol{\theta}_t) = 0$ if $\Gamma_\theta(\boldsymbol{\theta}_t) < \tau_\theta < 1$ where the threshold τ_θ is optimized during calibration stage.

Prediction stage. The prediction stage obtains the prior probability $\Pr[\mathbf{x}_t|\boldsymbol{\theta}_t, \mathbf{S}_{t-1}]$ of the target state based on the belief $\Gamma(\mathbf{x}_{t-1}|\boldsymbol{\theta}_t)$ at time $t-1$ and updates equation as

$$\Pr[\mathbf{x}_t = \mathbf{H}_i|\mathbf{r}_j, \mathbf{S}_{t-1}] = \sum_{q=0}^{N_H} \gamma_{i,q}^{(x)}(\mathbf{r}_j) \, \Gamma_{\mathrm{x}}(\mathbf{x}_{t-1} = \mathbf{H}_q|\mathbf{r}_j) \tag{11}$$

for any $\boldsymbol{\theta}_t = \mathbf{r}_j$ and where

$$\gamma_{i,q}^{(x)}(\boldsymbol{\theta}_t) = \Pr[\mathbf{x}_t = \mathbf{H}_i | \mathbf{x}_{t-1} = \mathbf{H}_q, \boldsymbol{\theta}_t] \tag{12}$$

is the target state transition probability for the model in Eq. (3). In the case study of Sect. III-C, we show how to efficiently exploit the knowledge of the prior probability given in Eq. (11) to provide a tentative estimation of the human motion intentions and to dynamically define the safety zones for robot interaction.

Update stage. The update stage computes the new mode-conditioned a-Posteriori probability $\Gamma(\mathbf{x}_t|\boldsymbol{\theta}_t)$ as

$$\Gamma_x(\mathbf{x}_t = \mathbf{H}_i|\boldsymbol{\theta}_t = \mathbf{r}_j) \propto \Pr(\mathbf{s}_t|\mathbf{H}_i, \mathbf{r}_j) \Pr[\mathbf{H}_i|\mathbf{r}_j, \mathbf{S}_{t-1}] \tag{13}$$

where prior pdf $\Pr[\mathbf{H}_i|\mathbf{r}_j, \mathbf{S}_{t-1}]$ is defined in Eq. (11), while $\Pr(\mathbf{s}_t|\mathbf{H}_i, \mathbf{r}_j)$ is the joint likelihood function that depends on the DFL model Eqs. (6) and (7) as

$$\begin{aligned} &\Pr(\mathbf{s}_t|\mathbf{H}_i, \mathbf{r}_j) = \textstyle\prod_{\ell \in \mathcal{L}_T} \Pr[s_{\ell,t}|h_\ell(\mathbf{H}_i|\mathbf{r}_j)] = \\ &= \textstyle\prod_{\ell \in \mathcal{L}_T} \lambda[h_\ell(\mathbf{H}_i|\mathbf{r}_j), \sigma_\ell(\mathbf{H}_i|\mathbf{r}_j)] \end{aligned} \tag{14}$$

with $\lambda(h_\ell, \sigma_\ell) = \frac{1}{(2\pi)^{1/2}\sigma_\ell} \exp\left\{-\frac{(s_{\ell,t}-h_\ell)^2}{2\sigma_\ell^2}\right\}$. The a-Posteriori probability $\Gamma_x(\mathbf{x}_t = \mathbf{H}_i)$ in Eq. (1) is updated at time t as $\Gamma_{\mathrm{x}}(\mathbf{H}_i) = \sum_j \Gamma_{\mathrm{x}}(\mathbf{H}_i|\mathbf{r}_j)\Gamma_\theta(\boldsymbol{\theta}_t = \mathbf{r}_j)$, where mode-conditioned probability $\Gamma_x(\mathbf{H}_i|\mathbf{r}_j)$ is defined in Eq. (13) and $\Gamma_\theta(\mathbf{r}_j)$ according to Eq. (2), respectively. Finally, MAP estimation

$$\widehat{\mathbf{x}}_t = \underset{\boldsymbol{x}_t \in \bar{\mathcal{H}}}{\operatorname{argmax}} \Gamma_x(\boldsymbol{x}_t) \tag{15}$$

is adopted for target state tracking.

B. Hidden Markov model based detection of robot activity

For the estimation of the current robot task, we now focus on the subset $\mathcal{L}_R \subseteq \mathcal{L}$ collecting the links $\ell \in \mathcal{L}_R$ that provide the best tradeoff between sensitivity to robotic arm movements and minimal RF wavefield distortion caused by the operator activity in the shared space. According to the constraint already introduced in Sect. II-A for $\mathcal{L}_T$, the subset $\mathcal{L}_R$ is selected according to the spatial constraint $\mathcal{L}_R = \{\ell \in \mathcal{L} : \forall i \in N_H,\ d_{\ell,i} > \Delta_{\text{op}}/2 + \rho_{\ell,\max}\}$ where $d_{\ell,i}$ is the distance of $\mathbf{H}_i$ *w.r.t.* the line-of-sight of the ℓ-th link and Δ_{op} is the target size along $d_{\ell,i}$. We considered $\Delta_{\text{op}} = 1$m even though this is a very conservative constraint (see Sect. III-C).

For the selected link $\ell \in \mathcal{L}_R$, the information about the robot state (or configuration) $\boldsymbol{\theta}_t$ at time t is embedded in the noisy RSS samples $s_{\ell,t} = s_{\ell,t}(\boldsymbol{\theta}_t|\mathbf{x}_t)$ that can be approximated by

$$s_{\ell,t} \approx h_{\ell,\mathrm{R}}(\mathbf{r}_j) + w_{\ell,\mathrm{R}}(\mathbf{r}_j) \tag{16}$$

where the deterministic term $h_{\ell,\mathrm{R}}$ is based on Eq. (6). It is computed by averaging out the distortions caused by the operator in any position $\mathbf{x}_t \in \bar{\mathcal{H}}$ (assumed as equiprobable)

$$\begin{aligned} &h_{\ell,\mathrm{R}}(\mathbf{r}_j) = \mathrm{E}_{\mathbf{x}_t}\left[h_\ell(\mathbf{x}_t|\mathbf{r}_j)\right] = \\ &= \tfrac{1}{N_H+1}\textstyle\sum_{\mathbf{x}_t\in\bar{\mathcal{H}}} h_\ell(\mathbf{x}_t|\mathbf{r}_j) = h_\ell(\mathbf{H}_0|\mathbf{r}_0) - \Delta h_{\ell,\mathrm{R}}(\mathbf{r}_j) \end{aligned} \tag{17}$$

where, as in Eq. (6), $\Delta h_{\ell,\mathrm{R}}(\mathbf{r}_j)$ is the additional average attenuation observed in the surroundings of the robotic arm carrying out task $\mathbf{r}_j$. The additional random log-normal fading term $w_{\ell,\mathrm{R}}$ now accounts for the residual fluctuations of RSS due to: *i*) the pre-defined movements of the robotic arm characterizing the state $\mathbf{r}_j$ and *ii*) the presence of the operator in the shared space. Therefore, it is $w_{\ell,\mathrm{R}}(\mathbf{r}_j) \sim N(0, \sigma^2_{\ell,\mathrm{R}}(\mathbf{r}_j))$ with $\sigma^2_{\ell,\mathrm{R}}(\mathbf{r}_j) = \mathrm{E}_{\mathbf{x}_t}\left[\left(s_{\ell,t}(\boldsymbol{\theta}_t|\mathbf{x}_t) - h_{\ell,\mathrm{R}}(\mathbf{r}_j)\right)^2\right]$ and

$$\sigma_{\ell,\mathrm{R}}(\mathbf{r}_j) = \sigma_\ell(\mathbf{H}_0|\mathbf{r}_0) + \Delta\sigma_{\ell,\mathrm{R}}(\mathbf{r}_j) \tag{18}$$

where $\Delta\sigma_{\ell,\mathrm{R}}(\mathbf{r}_j)$ is the increased RSS standard deviation.

Hidden Markov modeling (HMM) is adopted for iterative robot state tracking: the goal is to uncover the hidden robot task $\mathbf{r}_k$ at time t by maximizing the a-Posteriori probability $\Gamma_\theta(\boldsymbol{\theta}_t)$ over the link subset $\mathcal{L}_R$ where

$$\Gamma_\theta(\boldsymbol{\theta}_t = \mathbf{r}_k) \propto \Pr[\mathbf{s}_t|\mathbf{r}_k] \sum_{\mathrm{j}} \gamma^{(\theta)}_{k,j}\, \Gamma_\theta(\boldsymbol{\theta}_{t-1} = \mathbf{r}_j) \tag{19}$$

and the robot state transition $\gamma^{(\theta)}_{k,j}$ is defined in Eq. (4). Similarly, as shown in Eq. (14), the probability

$$\begin{aligned} &\Pr[\mathbf{s}_t|\mathbf{r}_k] = \textstyle\prod_{\ell\in\mathcal{L}_R} \Pr\left[s_{\ell,t}|h_{\ell,\mathrm{R}}(\mathbf{r}_k)\right] = \\ &= \textstyle\prod_{\ell\in\mathcal{L}_R} \lambda\left[h_{\ell,\mathrm{R}}(\mathbf{r}_k), \sigma_{\ell,\mathrm{R}}(\mathbf{r}_k)\right] \end{aligned} \tag{20}$$

indicates the likelihood function for the robot task state $\mathbf{r}_k$. It corresponds to the model shown in Eqs. (17) and (18).

C. Multiple model calibration and testing

The purpose of the multiple model calibration procedure is to obtain the DFL model parameters $\Delta h_\ell(\mathbf{H}_i|\mathbf{r}_j)$ and $\Delta\sigma_\ell(\mathbf{H}_i|\mathbf{r}_j)$ to be used for operator tracking in Eqs. (6) and (7), respectively. Moreover, calibration is also employed to acquire the HMM parameters used for robot task state detection $\Delta h_{\ell,\mathrm{R}}(\mathbf{r}_j), \Delta\sigma_{\ell,\mathrm{R}}(\mathbf{r}_j)$ in Eqs. (17) and (18).

A software tool automatically performs all steps of the calibration procedure, collecting RSS observations related to both operator and robot movements: for each robot task state $\mathbf{r}_j$, starting from $\mathbf{r}_0$, an operator moves along a predefined training path that spans all covered positions $\mathbf{H}_i$. In Fig. 1, $N_H = 24$ positions are considered while the first 12 positions are also highlighted for convenience. The sink node collects and synchronizes the RSS observations received from the wireless devices while these are used to evaluate the sample average $h_\ell(\mathbf{H}_i|\mathbf{r}_0)$ and the sample standard deviation $\sigma_\ell(\mathbf{H}_i|\mathbf{r}_0)$ for each link $\ell \in \mathcal{L}$ and for each position $i = 0, ..., N_H$. From these measurements, it is easy to compute the DFL parametric maps $\Delta h_\ell(\mathbf{H}_i|\mathbf{r}_j)$ and $\Delta\sigma_\ell(\mathbf{H}_i|\mathbf{r}_j)$. Finally, the calibration of the HMM parameters $\Delta h_{\ell,\mathrm{R}}(\mathbf{r}_j)$, $\Delta\sigma_{\ell,\mathrm{R}}(\mathbf{r}_j)$ for robot state detection is carried out by merging the RSS observations for each target position. In the case studies summarized in Sect. III-C, the calibration of each target-robot state pair ($\mathbf{H}_i$,$\mathbf{r}_j$) takes about 15 s while the whole calibration procedure takes about 30 minutes.

Fig. 3 shows the selected parametric model maps $\Delta h_\ell(\mathbf{H}_i|\mathbf{r}_j)$ and $\Delta\sigma_\ell(\mathbf{H}_i|\mathbf{r}_j)$ obtained from experimental data collected in the test plant of Sect. III. The experimental connectivity maps for average RSS $\Delta h_\ell(\mathbf{H}_i|\mathbf{r}_j)$ (Fig. 3-left) and standard deviation $\Delta\sigma_\ell(\mathbf{H}_i|\mathbf{r}_j)$ (Fig. 3-right) are depicted for an operator outside the detection area (*i.e.,* $\mathbf{H}_0$) and inside the shared workspace at positions $\mathbf{H}_1$, $\mathbf{H}_6$ and $\mathbf{H}_{12}$ (see the corresponding columns in the left and right part of Fig. 3). Different robot tasks are shown: the default position $\mathbf{r}_0$ (*i.e.,* first row), forward and backward translation $\mathbf{r}_1$ (*i.e.,* second row), left side roto-translation $\mathbf{r}_2$ (*i.e.,* third row) and, finally, right side rotation $\mathbf{r}_3$ (*i.e.,* fourth row). Each robot task takes approximately T_R = 360 ms. Background maps $h_\ell(\mathbf{H}_0|\mathbf{r}_0)$ and $\sigma_\ell(\mathbf{H}_0|\mathbf{r}_0)$ are also shown in the corresponding sub-figures (on top-left corner). The link subsets for operator tracking (green boxes $\mathcal{L}_T$) and robotic arm activity detection (blue boxes $\mathcal{L}_R$) are highlighted for each case.

III. Integration and validation of DFL systems in HRC industrial setups

In this section, we report the most critical issues of DFL system integration, first in terms of network deployment for an industrial HRC scenario (Sect. III-A), and then in terms of automation safety technology (Sect. III-B). Notably, we also introduce here the possibility to implement redundancy and fusion of inputs (*i.e.,* different sources of localization information) that will be detailed in Sec. IV-B with the intent to effectively balancing some less accurate location estimates and possibly slow refresh rates. Finally, we present here some DFL real-time accuracy results (Sect. III-C) obtained during some experimental field trials inside an industrial pilot plant.

A. Deployment of the DFL system

The DFL system is deployed in the setup of Fig. 1 by exploiting a pre-existing network of $\mathrm{N} = 15$ wireless nodes working in the 2.4 GHz ISM band. The DFL system monitors $L = 105$ bidirectional wireless links, whose length is in the distance range $1 < d_\ell < 10$ m and, therefore, with Fresnel radius limited in the range $18 < \rho_{\ell,\max} < 56$ cm depending on the corresponding value d_ℓ as described in Sect. II-A. The usage of the unlicensed 2.4 GHz ISM band and the IEEE802.15.4 standard [23] is motivated by the low cost and large availability of many HW platforms ready for customization. In the presented deployment, the following assumptions hold: first, the layout is static and cannot change over time, with the most

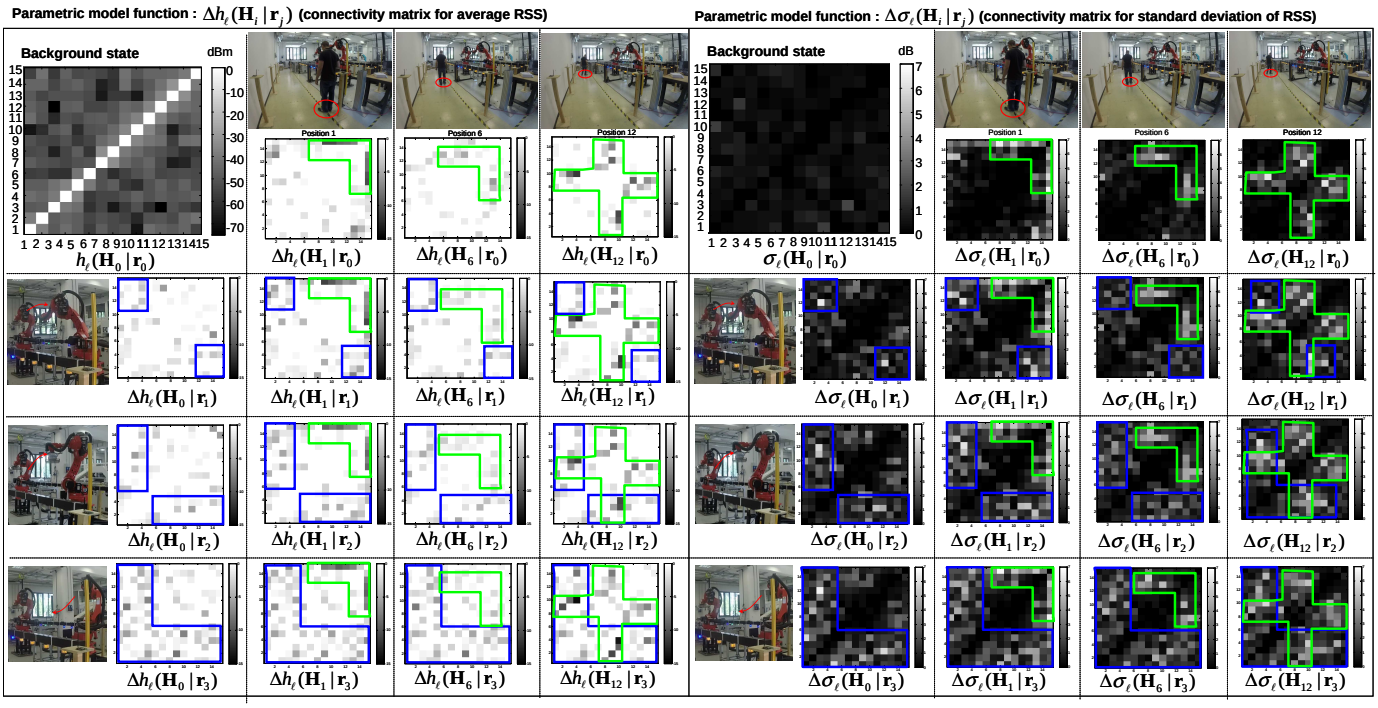

Fig. 3. IMM calibration testing: average RSS (left) and standard deviation (right) connectivity maps for an operator inside the shared workspace. Operator positions in columns: $\mathbf{H}_1$, $\mathbf{H}_6$, $\mathbf{H}_{12}$ and outside the detection area $\mathbf{H}_0$. Robotic arm states in rows: *i*) in the default position ($\mathbf{r}_0$, first row); *ii*) translating forward and backward ($\mathbf{r}_1$, second row), *iii*) roto-translating on the left side ($\mathbf{r_2}$, third row) and, finally, *iv*) rotating on the right side ($\mathbf{r_3}$, fourth row). The most sensitive link subsets to the operator movements (green boxes $\mathcal{L}_T$) and robot activity (blue boxes $\mathcal{L}_R$) are highlighted for the operator standing on position $\mathbf{H}_1$.

significant moving objects restricted to the robot (*i.e.,* R1) and the operator. Second, the industrial wireless network adopts both static calibration and standard compliant interference mitigation schemes. Third, the calibration procedure needs human intervention as the operator must physically occupy the positions of interest. Accurate electromagnetic simulation tools could be adopted for predicting the human-induced fading and limit the set-up time [24].

The purpose of this case study is to show the feasibility of DFL systems in industrial HRC settings, and to evaluate the performances of the proposed method for the relevant case of one-to-one human-robot interaction inside an industrial cell. Although not considered in the experimental study, multiple non-interfering DFL networks could be installed to cover larger areas (consisting of spatially separated cells). RF prediction tools, as well as dynamic interference mitigation schemes and the use of licensed bands are not discussed here but can be easily implemented in practical systems working in harsh RF environments.

The wireless devices are deployed along the perimeter of a convex area that includes the target workspace (see Fig. 1) in order to avoid unreliable links (*e.g.,* 3-nodes alignment) and occupation of walking areas. Devices periodically transmit data/control frames on every $\Delta t = 60$ ms, allowing for real-time acquisition of $L/\Delta t = 1750$ RSS measurements/s. This sampling interval is short enough for DFL processing to capture significant observations of robot tasks $\mathbf{r}_j$: for tasks of approximately $T_R = 360$ms each, $T_R/\Delta t = 6$ RSS consecutive samples are used to monitor the robotic arm and to refresh the estimated target state. The NC device (red node in Fig. 1 and 4) acts as the network manager and collects the set of L noisy measurements $\mathbf{s}_t$. Each wireless device module features a NXP JN5148 single chip micro-controller [25] that

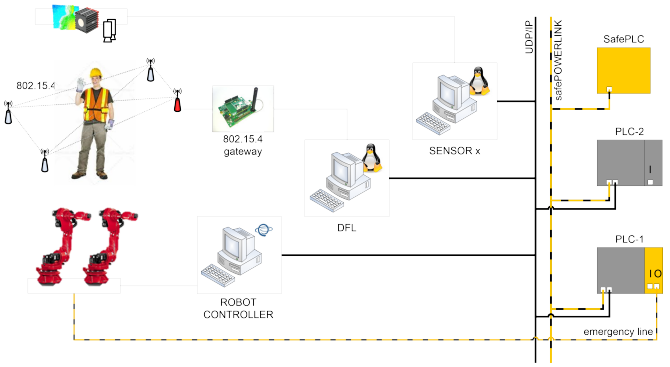

Fig. 4. System architecture with robots, multiple sources of human detection and a set of PLCs collectively encompassing the safety functions. Safety-rated CPU (SafePLC) and standard PLC (PLC-1/2) access both the safe fieldbus (safePOWERLINK) and regular channels (UDP/IP).

includes the RF circuitry. The RSS dynamic range for the chosen hardware is 75dB with a minimum sensitivity of about -95dBm. For all tests, we employed omnidirectional, vertically polarized antennas, with a gain of 2dBi, easily available as COTS and not requiring special alignments. RF nodes are configured to transmit with the transmit power set to 0 dBm.

B. Integration of the DFL system in a HRC safe architecture

Human tracking in HRC applications is part of the specific risk reduction measures [26] designed to maintain separation distances or monitoring the human body regions exposed to potential contacts. This is a safety function with normative requirements [3] in terms of functional safety. For the sensory subsystems, these requirements are partly satisfied by proce-

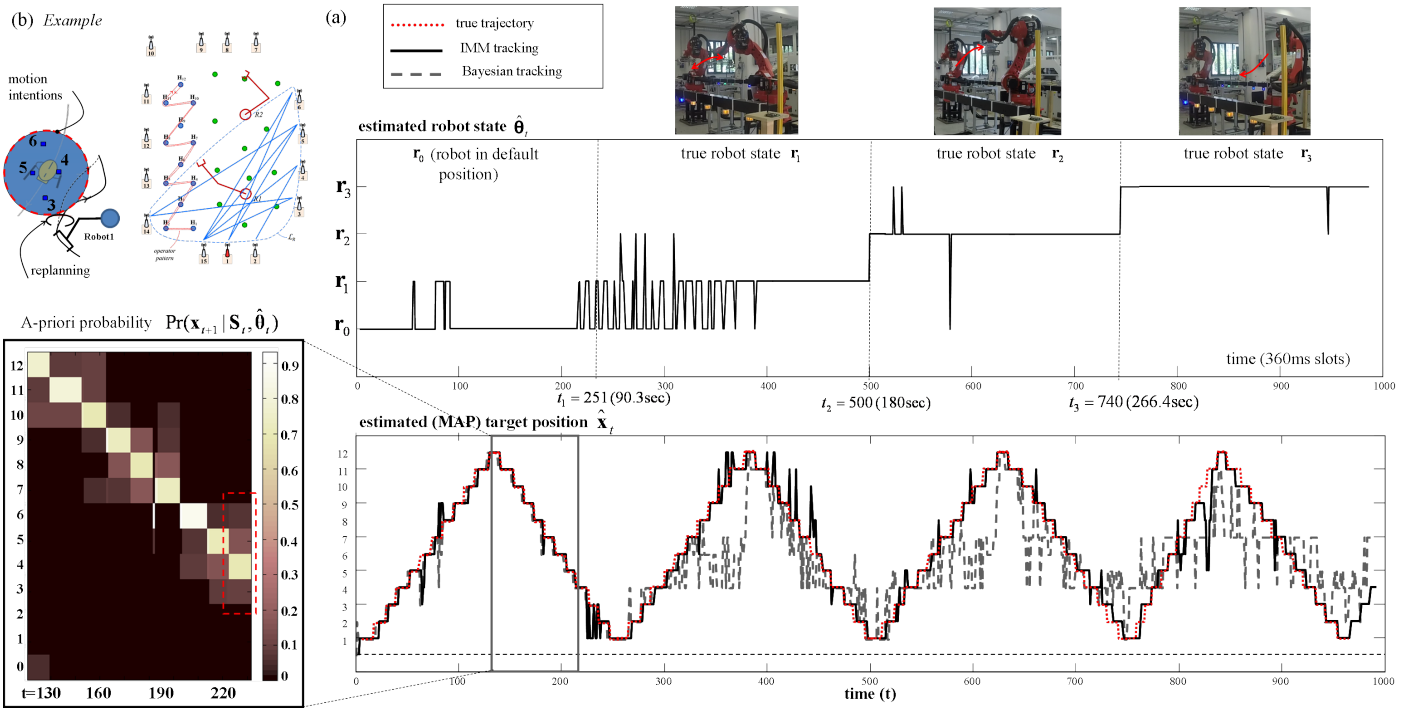

Fig. 5. (a) Experimental results for device-free tracking of an operator entering in and exiting from the detection area. Bottom chart: true (dashed red lines, see also the top-left corner sub-figure) and estimate (solid and dashed black lines) paths of the operator. The robot R1 activity during the tests can be described as the following sequence of states: $\mathbf{r}_0$ default position; $\mathbf{r}_1$ forward and backward translation, $\mathbf{r}_2$ left side roto-translation and, finally, $\mathbf{r}_3$ right side rotation. Middle-chart: robot state detection $\hat{\boldsymbol{\theta}}_t$ for the highlighted link subset $\mathcal{L}_R$ depicted above (blue links). (b) bottom: a-priori probability for a close-up time interval ($\approx$ 30 s). Top: safe area in the surroundings of position $\mathbf{H}_4$ (highlighted by dashed red lines), possibly triggering R1 replanning.

dures and architectures designed to reduce or eliminate the risk of undetected failures. First, the source of tracking data is duplicated: for the principle of diversity (as per ISO 13849), the DFL localization service is combined with a system of ceiling-mounted Time-of-Flight (ToF) cameras, available in the experimental setup (see Fig. 1 and 4). Second, both sensor subsystems are integrated within a safety framework [27] where any safety-relevant information is elaborated by multiple CPUs. Specifically, two standard Programmable Logical Controllers (PLCs) and safePLCs (B&R, Austria - see also Fig. 4) are interconnected by the safePOWERLINK protocol to deploy the capabilities of the safety functions. Third, data exchanged among sensors (*i.e.,* inputs) and PLCs (*i.e.,* logic) are implemented through monitored *black channels* (as introduced in IEC 62280-1), where intrinsically unsafe channels (*e.g.,* Ethernet) may, in fact, be used as a safety-unaware transport layer, on top of which a custom application layer implements methods for errors and data consistency checking. Each standard PLC is connected to each sensory subsystem via a UDP/IP protocol. Check methods include running number, time-stamping, timeout and hosts identifications for detecting packet losses, repetitions, insertions, delayed and incorrect sequences. A standard hashing function with shared key is used to check the data frame integrity.

As a result, a failsafe communication protocol is established among all wired nodes. In particular, the wired entry point for the DFL network is represented by a gateway node (near the red node in Fig. 4) that supports both data collection and RSS analytics for DFL processing. It is implemented on an ad-hoc wireless device that is physically separated from the NC and behaves as a sink node. As far as the wireless network is concerned, it is composed by RF nodes with modified MAC sub-layer, redesigned on top of the beacon-enabled mode of the standard IEEE 802.15.4 in order to manage RSS data collection. A detailed overview of the MAC design and the alternative implementation of the gateway on the NC are reported in [20].

By exploiting these computational units and protocols, the framework globally provides most of the elements of a Designated Category 3 architecture. On top of the cross-monitoring of input-logic-output functions, the proposed framework enables the real-time analysis of data in PLCs and provides any safety algorithm with vital information about latencies, delays, synchronization and other spatial inaccuracies (*i.e.,* mutual calibration). Such information and failsafe data are used in PLCs for target localization, *i.e.,* fusing together the DFL and the ToF channels (see Sec. IV-B).

C. Experimental results for real-time operator tracking

In the experimental sessions, we have addressed the problem of device-free tracking of an operator entering into and exiting from a shared detection area (see Fig. 1). The considered scenario is characterized by one human worker interacting with a single robotic manipulator for handling and assembling tasks inside a confined fenceless area. Therefore, the focus is on a typical HRC configuration but critical enough for industrial applications to stimulate an ad-hoc research. The manipulator R1 is programmed to perform a sequence of typical pick&place motion tasks that have been selected among the following ones: default configuration $\mathbf{r}_0$ (for 90.3 s), forward and backward translation $\mathbf{r}_1$ (for 89.7 s), left side roto-translating $\mathbf{r}_2$ (for 86.4 s) and, finally, right side rotation $\mathbf{r}_3$ (for 93.4 s). At any time t, the on-line estimation of the operator position $\mathbf{x}_t$ is based on

the knowledge of the 2D map set $\Delta h_\ell(\mathbf{H}_i|\mathbf{r}_j)$ and $\Delta\sigma_\ell(\mathbf{H}_i|\mathbf{r}_j)$ over link subset $\ell \in \mathcal{L}_T$ and $\Delta h_{\ell,\mathrm{R}}(\mathbf{r}_j)$, $\Delta\sigma_{\ell,\mathrm{R}}(\mathbf{r}_j)$ over link subset $\ell \in \mathcal{L}_R$ for instantaneous robot state detection (see Fig. 2). The localization performance observed from the experimental data is analyzed in Fig. 5. The operator moves sequentially (8 times) at a maximum speed of about 1 m/s from position $\mathbf{H}_1$ to $\mathbf{H}_{12}$ and then backward while standing in each position for a max. of 5 s (possibly moving and turning inside a small voxel of ground squared size $\Delta_{\mathrm{op}} = 1$ m). Fast variations of the true position vs. time (dotted red lines in Fig. 5.b) indicate the movement of the operator into a nearby reference location. In Fig. 5.a, the corresponding estimated locations of the target over time (solid and dashed lines) are compared with the true trajectory of the operator in the shared space. Performances of target tracking using the IMM approach are shown in solid lines, together with the MAP estimation of the robot state $\hat{\boldsymbol{\theta}}_t$ (10) acting as jump Markov parameter. Comparatively, performances of the tracking with standard Bayesian sequential estimation [14] without jump parameter is shown in dashed gray lines. The observed root mean square estimation error (RMSE) of target localization, defined as $\sigma = \sqrt{\mathrm{E}_t\left[\|\hat{\mathbf{x}}_t - \mathbf{x}_t\|^2\right]}$, is found to be about 0.15 m for IMM tracking and 0.35 m for Bayesian sequential estimation. The observed RMSE happens to be close to the error floor ($\approx 0.05 - 0.1$ m) due to the use of a discrete fixed grid of reference locations. The particle-filtering approach [14] can be also used to further improve the positioning performances without impacting too much on the estimation time.

In Fig. 5.b, we show also the related prior probability $\Pr[\mathbf{x}_{t+1}|\mathbf{S}_t, \hat{\boldsymbol{\theta}}_t]$ for a specific time interval: the operator is moving from position $\mathbf{H}_{12}$ located at the boundary of the workspace area towards position $\mathbf{x}_t = \mathbf{H}_4$ at time t, with robot switching from default position $\hat{\boldsymbol{\theta}}_t = \mathbf{r}_0$ to state $\mathbf{r}_1$. The prior probability $\Pr[\mathbf{x}_{t+1}|\mathbf{S}_t, \hat{\boldsymbol{\theta}}_t = \mathbf{r}_0]$ for the operator position at time $t+1$ provides an effective measure of the motion intentions and of the dynamic safety area size around the operator (for parametric threshold $0 < \tau < 1$) $\mathcal{S}_t := \left\{\mathbf{H}_i \in \overline{\mathcal{H}} \ : \ \Pr\left[\mathbf{x}_{t+1} = \mathbf{H}_i|\mathbf{S}_t, \hat{\boldsymbol{\theta}}_t\right] > \tau\right\}$. This information can be used for real-time evaluation of safety areas to allow fast robot re-planning activities [7]. In the same example of Fig. 5.b, for $\tau = 0.01$ the safety area around the operator in $\mathbf{x}_t = \mathbf{H}_4$ contains positions $\mathcal{S}_t \in \{\mathbf{H}_4, \mathbf{H}_5, \mathbf{H}_3, \mathbf{H}_6\}$ with corresponding probabilities $[0.6,\ 0.2,\ 0.15,\ 0.05]$, respectively.

IV. HRC Simulation Toolset and Performance Analysis

A simulation toolset has been developed to validate the accuracy of the proposed IMM tracking method with respect to *i*) randomly varying robot activity sequences, *ii*) arbitrary human movements, *iii*) other DFL methods proposed in previous works (Sect. IV-A), and *iv*) a fusion method with different sensing sources (see also Sect. IV-B). The toolset takes as input the operator trajectory, the sequence of programmed robot states/activities, and a training data-set (Sect. II-C) used to generate synthetic RSS sequences from the log-normal model shown in Eq. (5). The operator trajectories $\mathbf{x}_t$ are here simulated according to the model shown in Eq. (3) where the target is assumed to move randomly by covering the position set $\mathbf{x}_t \in \overline{\mathcal{H}}$ described in the previous section and depicted in Figs. 1 and 5.b. The movements of the target are simulated according to a 2D random walk mobility model

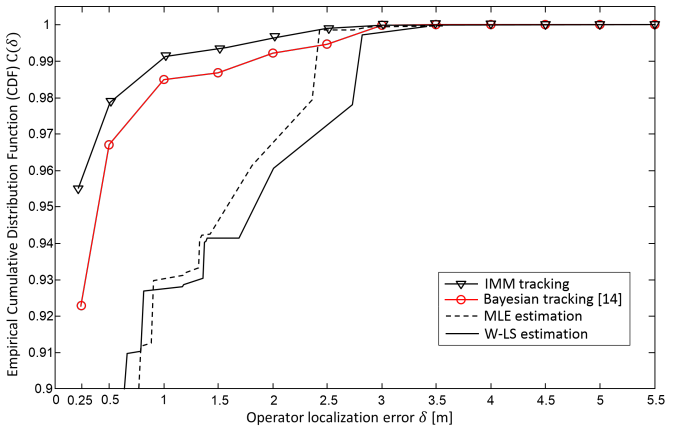

Fig. 6. Empirical CDF for localization error evaluation obtained from simulations: IMM method compared with Bayesian tracking, Maximum Likelihood Estimation (MLE) and Weighted Least-Squares (W-LS).

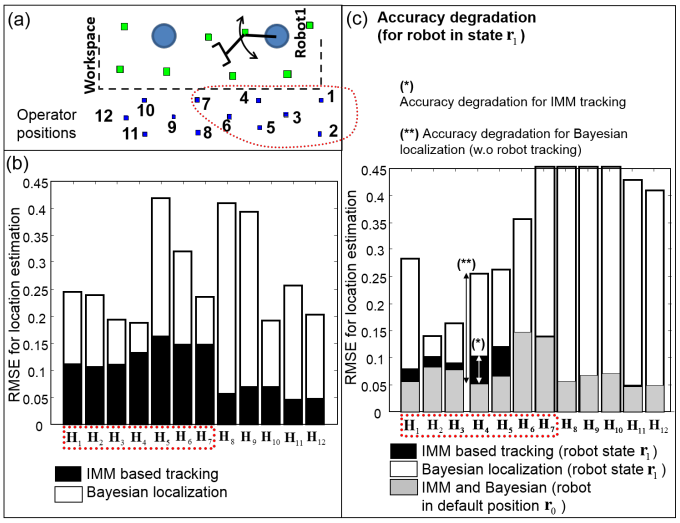

Fig. 7. Simulated device-free tracking performance for varying positions inside the shared space. (b) Comparative analysis between IMM and standard Bayesian tracking approaches (without Markovian jumps). (c) Accuracy degradation for IMM and standard Bayesian approach due to the change in the robot configuration from the default state $\mathbf{r}_0$ to the state $\mathbf{r}_1$.

[28] with Circular Gaussian random driving process $\mathbf{v}_t$ with deviation of 3 spatial samples that correspond to a maximum speed of 1 m/s. Similarly, the sequence of movements of the robotic arm is randomly generated from the state space $\mathbf{r}_j \in \bar{\boldsymbol{\Theta}}$ (including $\mathbf{r}_0$ corresponding to the robot in the default position). A new robot task is chosen every 30 s. For any pair of operator position $\mathbf{H}_i$ and robot state $\mathbf{r}_j$, synthetic RSS data are now generated by Monte Carlo simulations according to Eq. (5) with the parametric model maps $\Delta h_\ell(\mathbf{H}_i|\mathbf{r}_j)$ in Eq. (6) and $\Delta\sigma_\ell(\mathbf{H}_i|\mathbf{r}_j)$ in Eq. (7) observed during calibration. The likelihood functions corresponding to the simulated operator and robot patterns are modeled as in Eqs. (14) and (20), respectively.

Localization results in Figs. 6 and 7 are computed for long enough operator trajectories to uniformly cover all selected positions of the set $\overline{\mathcal{H}}$ and all sequences of robotic arm states of the set $\bar{\boldsymbol{\Theta}}$, corresponding to about 120 minutes of real-time simulation.

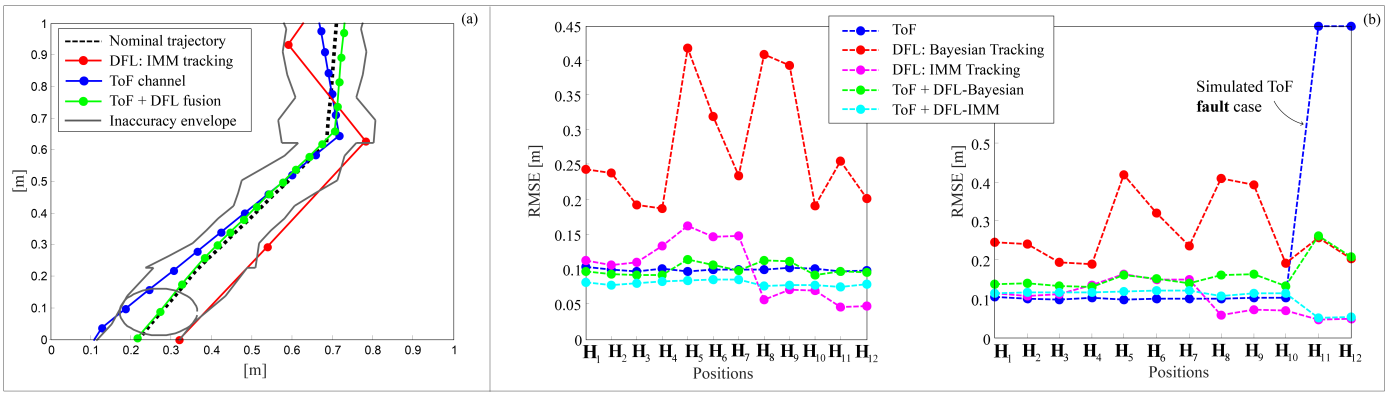

Fig. 8. (a) Example of an operator trajectory (2D projections): the simulated nominal trajectory (*i.e.,* dashed gray) is estimated by the DFL IMM (*i.e.,* red) and the ToF (*i.e.,* blue) channels only and by the sensor fusion (*i.e.,* green) one. Dots represent the actual estimates. At any time, the tracking uncertainty can be represented by a symmetric (circular) area around the estimates, enveloped (*i.e.,* gray boundary) along the path. (b) left: localization RMSE accuracy for ToF, DFL Bayesian, DFL IMM, fused ToF/DFL IMM, and fused ToF/DFL Bayesian channels for different positions inside the shared space. (b) right: effect of ToF faults on accuracy of fused channel corresponding to positions 11 and 12.

A. *Device-free localization accuracy*

In Fig. 6, we analyze the empirical cumulative density function (CDF) of localization error $\mathrm{C}(\delta) = \Pr\left[\|\widehat{\mathbf{x}}_t - \mathbf{x}_t\| \leq \delta\right]$ and compare the performance of the IMM method with conventional location estimation schemes, namely Bayesian tracking, Maximum Likelihood Estimation (MLE) and weighted Least-Squares (W-LS), see [14],[16] for a review. For W-LS, the target location is estimated as

$$\widehat{\mathbf{x}}_t = \underset{\mathbf{H}_m \in \bar{\mathcal{H}}}{\operatorname{argmin}} \|\mathbf{s}_t - \mathbf{h}_{\mathrm{T}}(\mathbf{H}_m)\|_{\mathbf{C}_{\mathrm{T}}^{-1}(\mathbf{H}_m)} \tag{21}$$

where norm $\|\mathbf{s}\|_{\mathbf{C}_{\mathrm{T}}^{-1}} = \mathbf{s}^T \mathbf{C}_{\mathrm{T}}^{-1} \mathbf{s}$. Vector $[\mathbf{h}_{\mathrm{T}}(\mathbf{H}_m)]_{\ell \in \mathcal{L}_T} = h_{\ell,\mathrm{T}}(\mathbf{H}_m)$ with $h_{\ell,\mathrm{T}}(\mathbf{H}_m) = \mathrm{E}_{\boldsymbol{\theta}_t \in \bar{\boldsymbol{\Theta}}}\left[h_\ell(\mathbf{H}_m|\boldsymbol{\theta}_t)\right]$ and covariance $\mathbf{C}_{\mathrm{T}}(\mathbf{H}_m) = \operatorname{diag}\left[\boldsymbol{\sigma}_{\mathrm{T}}^2(\mathbf{H}_m)\right]$ with $\left[\boldsymbol{\sigma}_{\mathrm{T}}^2(\mathbf{H}_m)\right]_{\ell \in \mathcal{L}_T} = \sigma_{\ell,\mathrm{T}}^2(\mathbf{H}_m) = \mathrm{E}_{\boldsymbol{\theta}_t \in \bar{\boldsymbol{\Theta}}}\left[\left(\mathrm{s}_{\ell,t}(\boldsymbol{\theta}_t|\mathbf{H}_m) - \mathrm{h}_{\ell,\mathrm{T}}(\mathbf{H}_m)\right)^2\right]$ are functions of the parametric model maps obtained during the calibration stage and average out the distortions caused by the robotic manipulator in any state $\boldsymbol{\theta}_t \in \bar{\boldsymbol{\Theta}}$. The MLE criterion is instead defined as

$$\widehat{\mathbf{x}}_t = \underset{\mathbf{H}_m \in \bar{\mathcal{H}}}{\operatorname{argmax}} \Pr(\mathbf{s}_t|\mathbf{H}_m), \tag{22}$$

now with $\Pr(\mathbf{s}_t|\mathbf{H}_m) = \prod_{\ell \in \mathcal{L}_T} \lambda\left[h_{\ell,\mathrm{T}}(\mathbf{H}_m), \sigma_{\ell,\mathrm{T}}(\mathbf{H}_m)\right]$ indicating the likelihood function for the operator at position $\mathbf{H}_m$. The MLE and W-LS localization methods show significant performance degradation as neither robot nor operator state tracking are supported. As expected, the Bayesian technique provides accuracy improvements with respect to ML and W-LS as leveraging on a-priori information about the target motion. Observed localization errors are above 0.2 m with probability 10% for Bayesian localization and higher for ML and W-LS methods. On the contrary, the use of IMM joint tracking of operator and robot states guarantees an estimation error below 0.2 m with probability above 95%.

In Fig. 7.b, the RMSE performances of the proposed IMM tracking (*i.e.,* dark bars) and the Bayesian approach (*i.e.,* white bars) are now compared for the selected operator positions of Fig. 7.a. Target localization accuracy inside the highlighted position sub-set $\{\mathbf{H}_i\}_{i=1}^{7}$ is penalized with respect to the remaining ones. However, as also confirmed by the experimental case study, for these critical positions, the use of IMM tracking guarantees an estimation RMSE below 0.2 m. Instead, Bayesian localization experiences significant performance degradation with RMSE values above 0.4 m for some cases.

To isolate the accuracy degradation caused by the robotic arm movements, in Fig. 7.c, we have compared the localization accuracy observed for the robot in the default state (*i.e.,* grey bars) with the one observed for the robot in the active state $\mathbf{r}_1$. IMM tracking (*i.e.,* dark bars) and standard Bayesian localization (*i.e.,* white bars) are compared. Performance degradation of IMM tracking is limited to a RMSE increase of about 25% (on average) over positions $\mathbf{x}_t \in \{\mathbf{H}_i\}_{i=1}^{7}$ and negligible degradation in the remaining positions. On the contrary, the accuracy of the Bayesian technique is penalized over all positions (as blind with respect to robot movements), including those located far away from the robotic arm $\{\mathbf{H}_i\}_{i=8}^{12}$.

B. *Accuracy with practical sensor fusion approaches*

The architecture introduced in Sec. III-B, with the purpose of ensuring the functional safety of the sensory component, makes two failsafe channels available. As far as the evaluation of the proposed sensor fusion method is concerned, the joint use of two different channels is evaluated and compared here in terms of tracking accuracy. The two channels, namely the DFL channel from the DFL system and the ToF one from the camera vision system (see Sect. III-B), perform very differently in terms of sample rate, stand-alone accuracy and repeatability. However, the use of sensor fusion techniques is an effective solution to improve the localization accuracy by mitigating the negative effects that would be introduced by both sources if considered separately. In addition, the joint accuracy can be effectively upper-bounded by uncertainty regions of predictable size that can be used as dynamic safety areas for human-robot Separation Monitoring [5].

The fused target localization system exploits a standard Extended Kalman Filtering (EKF) system as the one described in [29] where the prediction of human motion is described according to the 2-D random walk mobility model shown in [28]. The update step of the predictor is implemented as an Indirect Filter, which simply merges the fusing sources without pre-filtering and/or feedforwarding/feedbacking steps. The filter covariance provides the inaccuracy of the target

location estimation. As a result, the EKF filter can supply synchronous output, *i.e.,* it can be implemented as part of the safety function in a failsafe real-time unit.

In Fig. 8.a, an example of an operator trajectory (*i.e.,* dotted gray line) is generated inside an area of the HRC workspace covered by both DFL and ToF camera sources. The trajectory simulation is based on the same assumptions described in the previous Sect. IV. The estimated position, after sensor fusion, is depicted in green, together with the boundary envelope (*i.e.,* gray) corresponding to the 95% confidence interval around the estimated operator location. The estimated operator trajectory is also compared with the trajectories obtained using the two channels separately. The noisy location estimates by the ToF channel are simulated according to their measured RMSE values; these values, in the range of $0.08-0.12$ m, are location dependent according to the ToF positions and their distances from the target locations inside the shared area. The estimates provided by the DFL channel are obtained from the IMM-based simulations of Sect. IV-A, whose results are also shown in Fig. 6 and 7. According to the industry-standard camera vision system employed in the real test plant, the ToF channel is configured with a sample interval equal to $T_{\text{ToF}} = 60$ ms. The fused estimates of the operator position, together with the corresponding uncertainty area, can be used to compute safety distances [7].

Fig. 8.b summarizes the localization accuracy (left sub-figure) of the proposed DFL IMM algorithm (*i.e.,* dashed magenta line) compared with the DFL Bayesian (*i.e.,* dashed red line) and the ToF (*i.e.,* dashed blue line) methods for different target positions inside the shared space. In addition, the performances of the sensor fusion algorithms ToF+DFL IMM (*i.e.,* dashed cyan line) and ToF+DFL Bayesian (*i.e.,* dashed green line) are presented, too. Compared with the results of the DFL system, the performances of the ToF system are almost location independent, while the best performances (*i.e.,* accuracy less than 0.1 m) are obtained for the fusion algorithm that exploits both ToF and DFL IMM channels.

Right-side sub-figure considers an industry-relevant case where the ToF system introduces some position-dependent errors (*e.g.,* over target positions 11 and 12) modelling a fault in some ToF devices or unsufficient/low visual area coverage. In this scenario, it can be shown that the availability of a alternative/backup source (*i.e.,* the DFL channel) and a sensor fusion algorithm can effectively limit the impairments introduced by the defective vision system.

V. Concluding remarks and future development

This paper proposes the use of DFL techniques as devised to contribute to the worker sensing ecosystem in human-robot cooperative (HRC) industrial spaces. The DFL system makes use of a pre-existing distributed wireless communication infrastructure for standard machine-to-machine (M2M) communication applications in industrial plants. The experimental case study focuses on the development and integration of DFL technologies for real-time location tracking of a human worker sharing the workspace with a robot manipulator. An IMM method is proposed to jointly track operator and robot movements and compared with conventional sequential estimation schemes. A simulator toolset has been also developed as a generalized design enviroment for localization accuracy prediction in arbitrary HRC environments, accounting for critical human-robot operational activities. The major impact for safety and context-aware human-centric robot technologies is due to the availability of a novel, non-invasive and dynamic human sensing approach, supporting the real-time localization of an operator w.r.t. the robot movements. Such new source is devised to enrich the range of safety sensors, which currently are the key-point of safe HRC solutions. In particular, the DFL system is able to provide a source of target information to be possibly fused with other sensor sources *e.g.,* environmental cameras, if available. Despite some highlighted issues that need to be considered as the objective for future research activities, experimental tests inside a pilot plant show that the proposed method is suitable to correctly detect the operator positions in real-time. The resulting position estimate can, for instance, be used for computing trajectory-dependent dynamic safety areas around either the robot or the operator.

References

[1] J. Krüger, T. Lien, and A. Verl, "Cooperation of human and machines in assembly lines," *CIRP Annals - Manufacturing Technology*, vol. 58, no. 2, pp. 628 – 646, 2009.

[2] L. Wang, "Collaborative robot monitoring and control for enhanced sustainability," *The International Journal of Advanced Manufacturing Technology*, pp. 1–13, 2013.

[3] ISO, *ISO 10218-2:2011: Robots and robotic devices – Safety requirements for industrial robots – Part 2: Robot systems and integration*. Geneva, Switzerland: International Organization for Standardization, 2011.

[4] J. Fryman and B. Matthias, "Safety of industrial robots: From conventional to collaborative applications," in *Robotics; Proceedings of ROBOTIK 2012; 7th German Conference on*, May 2012, pp. 1–5.

[5] ISO, *ISO/DTS 15066:2015: Robots and robotic devices – Collaborative robots*. Geneva, Switzerland: International Organization for Standardization, draft.

[6] T. Salmi, O. Väätäinen, T. Malm, J. Montonen, and I. Marstio, "Meeting new challenges and possibilities with modern robot safety technologies," in *Enabling Manufacturing Competitiveness and Economic Sustainability*, M. F. Zaeh, Ed. Springer International Publishing, 2014, pp. 183–188.

[7] F. Vicentini, N. Pedrocchi, M. Giussani, and L. Molinari Tosatti, "Dynamic safety in collaborative robot workspaces through a network of devices fulfilling functional safety requirements," in *ISR/Robotik 2014; 41st International Symposium on Robotics; Proceedings of*. VDE, 2014, pp. 1–7.

[8] N. Patwari, J. Ash, S. Kyperountas, A. Hero, R. Moses, and N. Correal, "Locating the nodes: cooperative localization in wireless sensor networks," *Signal Processing Magazine, IEEE*, vol. 22, no. 4, pp. 54–69, July 2005.

[9] J. Wilson and N. Patwari, "Radio tomographic imaging with wireless networks," *Mobile Computing, IEEE Transactions on*, vol. 9, no. 5, pp. 621–632, May 2010.

[10] S. Petersen and S. Carlsen, "WirelessHART Versus ISA100.11a: The Format War Hits the Factory Floor," *Industrial Electronics Magazine, IEEE*, vol. 5, no. 4, pp. 23–34, Dec 2011.

[11] N. Patwari and J. Wilson, "RF Sensor Networks for Device-Free Localization: Measurements, Models, and Algorithms," *Proceedings of the IEEE*, vol. 98, no. 11, pp. 1961–1973, Nov 2010.

[12] Y. Kilic, H. Wymeersch, A. Meijerink, M. Bentum, and W. Scanlon, "Device-free person detection and ranging in uwb networks," *Selected Topics in Signal Processing, IEEE Journal of*, vol. 8, no. 1, pp. 43–54, Feb 2014.

[13] M. Bocca, O. Kaltiokallio, N. Patwari, and S. Venkatasubramanian, "Multiple target tracking with rf sensor networks," *Mobile Computing, IEEE Transactions on*, vol. 13, no. 8, pp. 1787–1800, Aug 2014.

[14] S. Savazzi, M. Nicoli, F. Carminati, and M. Riva, "A Bayesian approach to Device-Free Localization: Modeling and experimental assessment," *Selected Topics in Signal Processing, IEEE Journal of*, vol. 8, no. 1, pp. 16–29, Feb 2014.

[15] S. Shi, M. Scholz, M. Beigl, Y. Ji, and S. Sigg, "Rf-sensing of activities from non-cooperative subjects in device-free recognition systems using ambient and local signals," *IEEE Transactions on Mobile Computing*, vol. 13, no. 4, pp. 907–920, 2014.

[16] A. Saeed, A. Kosba, and M. Youssef, "Ichnaea: A low-overhead robust wlan device-free passive localization system," *Selected Topics in Signal Processing, IEEE Journal of*, vol. 8, no. 1, pp. 5–15, Feb 2014.

[17] V. Jilkov and X. Li, "Online Bayesian estimation of transition probabilities for Markovian jump systems," *Signal Processing, IEEE Transactions on*, vol. 52, no. 6, pp. 1620–1630, June 2004.

[18] ISO, *ISO 13849-1:2006: Safety of machinery – Safety-related parts of control systems – Part 1: General principles for design*. Geneva, Switzerland: International Organization for Standardization, 2006.

[19] D. Izadi, J. Abawajy, and S. Ghanavati, "An alternative node deployment scheme for wsns," *Sensors Journal, IEEE*, vol. 15, no. 2, pp. 667–675, Feb 2015.

[20] V. Rampa, F. Vicentini, S. Savazzi, N. Pedrocchi, M. Ioppolo, and M. Giussani, "Safe Human-Robot Cooperation through Sensor-less Radio Localization," in *Industrial Informatics (INDIN), 2014 10th IEEE International Conference on*, July 2014.

[21] M. Hofbaur and B. Williams, "Hybrid estimation of complex systems," *Systems, Man, and Cybernetics, Part B: Cybernetics, IEEE Transactions on*, vol. 34, no. 5, pp. 2178–2191, Oct 2004.

[22] V. Rampa, S. Savazzi, M. Nicoli, and M. D'Amico, "Physical modeling and performance bounds for device-free localization systems," *Signal Processing Letters, IEEE*, vol. 22, no. 11, pp. 1864–1868, Nov 2015.

[23] "IEEE Standard for Local and metropolitan area networks–Part 15.4: Low-Rate Wireless Personal Area Networks (LR-WPANs) Amendment 1: MAC sublayer," *IEEE Std 802.15.4e-2012 (Amendment to IEEE Std 802.15.4-2011)*, pp. 1–225, April 2012.

[24] A. Eleryan, M. Elsabagh, and M. Youssef, "Synthetic generation of radio maps for device-free passive localization," in *Global Telecommunications Conference (GLOBECOM 2011), 2011 IEEE*, Dec 2011, pp. 1–5.

[25] NXP Laboratories (UK), "Data-sheet JN-DS-JN5148-001, IEEE 802.15.4 Wireless Microcontroller JN5148-001."

[26] ISO, *ISO 12100:2010: Safety of machinery – General principles for design – Risk assessment and risk reduction*. Geneva, Switzerland: International Organization for Standardization, 2010.

[27] F. Vicentini, N. Pedrocchi, and L. Molinari Tosatti, "SafeNet of Unsafe Devices-Extending the Robot Safety in Collaborative Workspaces," in *ICINCO (2)*, 2013, pp. 276–283.

[28] K.-H. Chiang and N. Shenoy, "A 2-d random-walk mobility model for location-management studies in wireless networks," *Vehicular Technology, IEEE Transactions on*, vol. 53, no. 2, pp. 413–424, March 2004.

[29] A. Mutambara, "Information based estimation for both linear and nonlinear systems," in *American Control Conference, 1999. Proceedings of the 1999*, vol. 2, Jun 1999, pp. 1329–1333 vol.2.